Computational and Theoretical Chemistry 984 (2012) 142–147

Contents lists available at SciVerse ScienceDirect

Computational and Theoretical Chemistry

journal homepage: www.elsevier.com/locate/comptc

Structural prediction of $(Au_{20})_N$ (N = 2–40) clusters and their building-up principle

Lei Ren, Longjiu Cheng *

School of Chemistry and Chemical Engineering, Anhui University, Hefei, Anhui 230039, People's Republic of China

ARTICLE INFO

Article history:
Received 9 October 2011
Received in revised form 16 December 2011
Accepted 15 January 2012
Available online 24 January 2012

Keywords:
Au_{20}
Molecular clusters
Multiple-center Lennard-Jones
Global optimization
Basin-hopping

ABSTRACT

We located the geometric structures of $(Au_{20})_N$ (N = 2–40) clusters using the basin-hopping method and multiple-center Lennard-Jones model potential. Some magic number structures have been observed, among which $(Au_{20})_5$ is a close-shell five-membered ring, $(Au_{20})_{20}$ is a hollow-cage, and $(Au_{20})_{35}$ is a double-cage in which the two cages share a five-membered ring. Moreover, the building-up principle of $(Au_{20})_N$ clusters is significantly different from that of the other molecular or atomic clusters. The orientational effect on Au_{20}–Au_{20} potential is much greater compared to that on C_{60}–C_{60} potential.

1. Introduction

Recently, more and more chemists and physicists have been paying their attention to studying gold nanoparticles and clusters due to the fact that they possess interesting properties that can be exploited for applications in catalysis [1–4] and biology [5]. With the purpose of understanding the peculiar properties of gold nanoparticles, a large number of research on gold clusters [6–14] using different theoretical methods were carried out, and a series of fascinating atomic structures have been observed. Gold neutral clusters Au_N display remarkable planar structures up to N = 6–9 [14,15], flat cages at N = 10–16 [14,16], hollow cages for N = 17–18 [16], Au_{20}: a tetrahedral pyramid [8,13,17], hollow-tubular structures dominate the low-lying population between Au_{21} and Au_{24} [18], a highly symmetric tube-like cage for Au_{26} [19], and Au_{32} showed a 24-carat golden fullerene [11,20]. Meanwhile, a lot of experimental techniques have been used to provide structural information for gold clusters, such as photoelectron spectroscopy [7,13,20], and infrared vibrational spectroscopy [9,21,22].

Au_{20} molecule exhibits novel structure and properties. First of all, Au_{20} molecule exhibits a unique tetrahedral structure with T_d symmetry, which has three different types of atoms, 4 at the apexes, 4 at the center of the surface, and 12 along the edges (as shown in Fig. 1). The stable anion of Au_{20} (T_d) holds its parent tetrahedral symmetry features a high catalytic activity [8]. Au_{20} has a very high surface area (all atoms are on the surface). Secondly, Au_{20} is a stable magic number. Photoelectron spectroscopy [13] suggests that Au_{20} molecules should be highly stable despite the fact that the crystal has not been achieved. The gap between highest occupied molecular orbit (HOMO) and lowest unoccupied molecular orbit (LUMO) even slightly exceeds that of the fullerene C_{60} molecule [8,13], which suggests that Au_{20} should be chemically very inert. Lots of attention has been focused on hollow cage golden nanoparticles, because the golden fullerenes have some features (for example, the capability of endo-bonding) of the classical carbon fullerenes [23,24]. Both Au_{20} and C_{60} are very eye-catching molecules. A lot of studies on C_{60} fullerenes focus on their complexes and packing styles of $(C_{60})_N$ clusters. The unusual short-ranged interaction determines the decahedral, tetrahedral, and close-packed motifs of the $(C_{60})_N$ clusters [25–27]. However, for Au_{20}, little attention has been devoted to structures of $(Au_{20})_N$ clusters, but to properties and compounds of Au_{20} molecule. How tetrahedral Au_{20} molecules pile together? What the structures of $(Au_{20})_N$ clusters look like? Is the packing of $(Au_{20})_N$ clusters similar to $(C_{60})_N$ clusters?

To answer above questions, we located the global minimum structures of $(Au_{20})_N$ clusters for N = 2–40 with multiple-center Lennard-Jones (MCLJ) potential using basin-hopping [28] method. Some magic number structures are obtained. The building-up principle of $(Au_{20})_N$ clusters is significantly different from that of the other molecular or atomic clusters. Moreover, the orientational effect of tetrahedral Au_{20} molecule on Au_{20}–Au_{20} potential is much greater than that of C_{60} molecule on C_{60}–C_{60} potential, which leads to the structures of $(Au_{20})_N$ clusters very different from those of $(C_{60})_N$ clusters.

* Corresponding author. Tel.: +86 551 5107342.
E-mail address: clj@ustc.edu (L. Cheng).

2210-271X/$ - see front matter Crown Copyright © 2012 Published by Elsevier B.V. All rights reserved.
doi:10.1016/j.comptc.2012.01.024

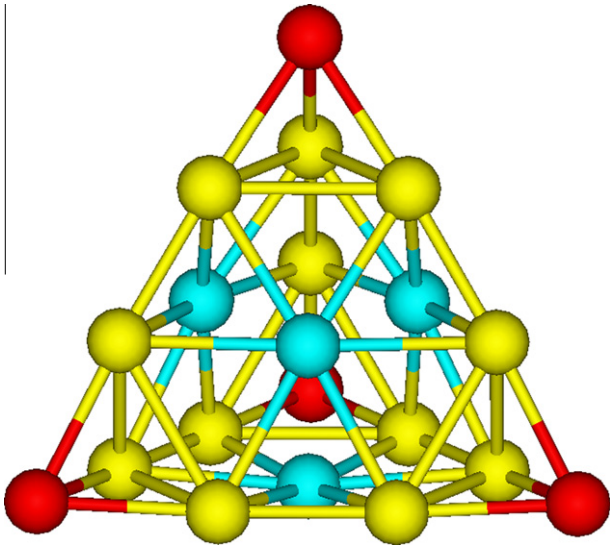

Fig. 1. The structure of Au_{20} molecule.

2. Theory and method

2.1. Potentials

Similar to that of the studies of $(C_{60})_N$ molecular clusters [25,29], the MCLJ potential is used to describe the interaction between Au_{20} molecules. In such a MCLJ model, Au_{20} molecules are taken as rigid bodies and only the Au–Au van der Waals interactions between different Au_{20} molecules are concerned. The Au–Au van der Waals interactions are described via an atomistic Lennard-Jones (LJ) pair potential, in the form:

$$\mathrm{LJ}(r) = 4 \cdot \varepsilon_{\mathrm{Au-Au}} \left[\left(\frac{\sigma_{\mathrm{Au-Au}}}{r} \right)^{12} - \left(\frac{\sigma_{\mathrm{Au-Au}}}{r} \right)^{6} \right]$$

where r is the distance between two atoms, and the LJ parameters, $\varepsilon_{\mathrm{Au-Au}} = 0.65$ kJ/mol, $\sigma_{\mathrm{Au-Au}} = 3.2$ Å, are fitted from first principle calculations [30]. Then the energy between any two Au_{20} molecules α and β is written as:

$$V^{\alpha\beta} = \sum_{i=1}^{20} \sum_{j=1}^{20} \mathrm{LJ}\left(r_{ij}^{\alpha\beta}\right)$$

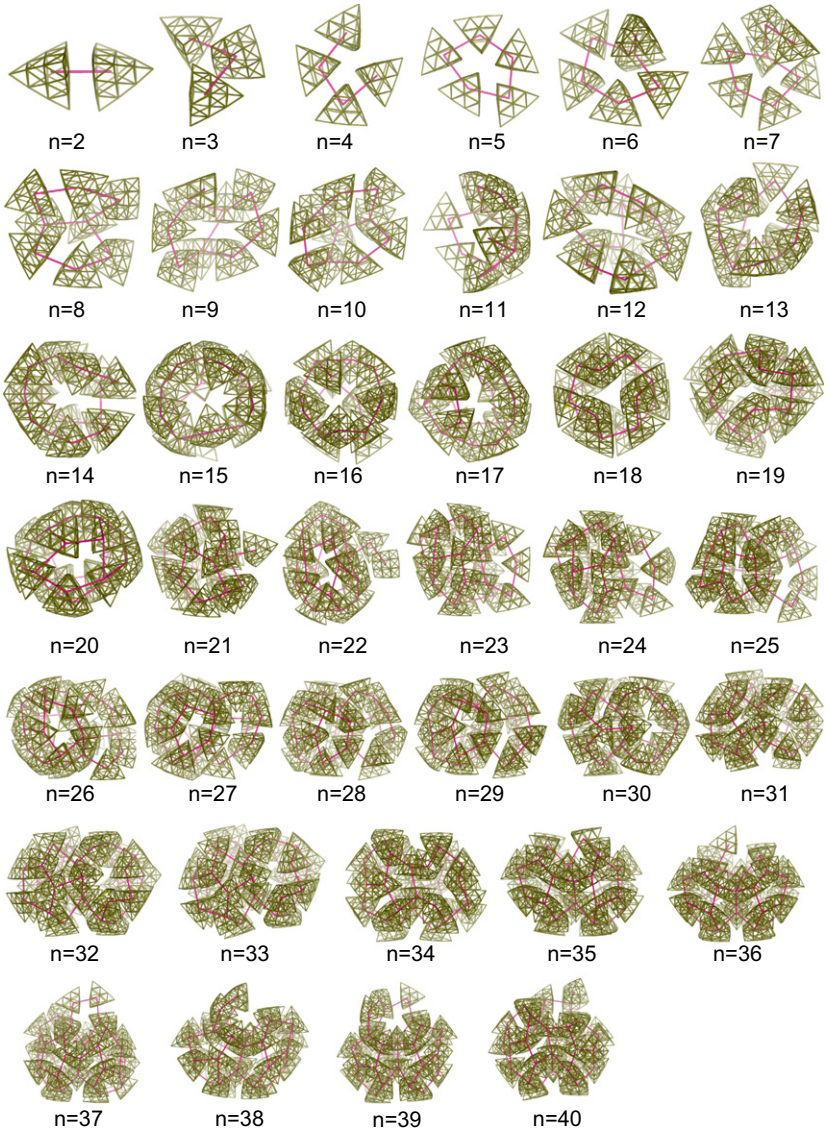

Fig. 2. The global minimum structures for $(Au_{20})_N$ clusters: $N = 2$–40. Red sticks represent the nearest-neighbor interaction.

where $r_{ij}^{\alpha\beta}$ represents distance between atom i in molecule α and atom j in molecule β.

2.2. Global optimization method

We performed a global-minimum search for the lowest energy $(Au_{20})_N$ clusters in the size range of $N = 2$–40 with MCLJ potential using the basin-hopping method. Basin-hopping or Monte-Carlo minimization is so far the most reliable algorithm in chemical and physics to search for the lowest-energy structure of atomic clusters and macromolecular systems [28,31–34], which has been previously used to search for lowest energy structures of LJ clusters [28], protein [35] and metal clusters [16,36].

3. Results and discussion

3.1. Global minimum structures

The located lowest-energy structures of $(Au_{20})_N$ ($N = 2$–40) clusters and their nearest-neighbor interaction (NN) are presented in Fig. 2. In the global minimum structure of $(Au_{20})_2$ cluster, to have more Au–Au LJ nearest-neighbor interactions, the two tetrahedral molecules are in face-to-face orientation (such a face-to-face interaction is defined as nearest-neighbor Au_{20}–Au_{20} interaction). The energy of global minimum $(Au_{20})_2$ is −25.506 kJ/mol, which is about 39 times of Au–Au LJ interaction (ε_{Au-Au}). In $(Au_{20})_3$, the center Au_{20} molecule is connected with the other two molecules via face-to-face interactions (the number of NN is 2). Similarly, $(Au_{20})_4$ has three nearest-neighbor interactions. The first close-shell structure is $(Au_{20})_5$, in which the five molecules form a five-membered ring, and the number of NN is five. Then $(Au_{20})_8$ is the next close-shell structure, in which the eight molecules form two five-membered rings. With such a growth pattern, $(Au_{20})_{15}$ is a lotus-form structure, $(Au_{20})_{20}$ is a hollow-cage (just like a seriously distorted dodecahedron with 12 five-membered rings), and $(Au_{20})_{35}$ is a double-cage where the two balls share a five-membered ring.

The energies of the located global minimum structures and the number of the nearest-neighbor interaction are given in Table 1. To show the relative stability of the global minimum structures at different cluster size, the energies are depicted in Fig. 3 in a manner that emphasizes particular stable minima or "magic numbers". Fig. 3a plots the gap between the energy and the "average" energy as a function of cluster size, where the "average" energy is a four-parameter fits of the energy curve. In such a curve, downward peaks represent that the energy is lower than the average and the structure is the most stable magic number ($N = 5$, 18–20, 33, 35 as shown in the figure). Moreover, Fig. 3b plots the second finite differences of energy $\Delta_2E = 2E_N - (E_{N+1} + E_{N-1})$, as a function of N. In which, we can also get some magic numbers at $N = 5$, 8, 10, 12, 16, 18, 23, 27, 30, 33, 35. At the magic numbers, the structures generally have a close shell of five-membered rings, and the number of NN is relatively more than that of the neighbors. But $(Au_{20})_{16}$ is an exception, which is not close-shell in five-membered rings but is most spherical, and so is a magic number too. Fig. 4 plots the detailed structures of $(Au_{20})_5$, $(Au_{20})_{18}$, $(Au_{20})_{20}$ and $(Au_{20})_{35}$, which display very notable packing, especially for $(Au_{20})_{18}$, which is a spherical hollow-cage with two sides open. There size range is about 2.1–3.4 nm as labeled in the figure.

3.2. Build-up principle

For most of the known cluster systems, such as LJ clusters [37], Morse clusters [38–40], modified Morse clusters [41,42], $(C_{60})_N$ clusters [25,27,43,44], and metal clusters [45,46], the packing styles are icosahedral, decahedral, and close-packed. However, the build-up principle of $(Au_{20})_N$ is much unexpected. In icosahedral, decahedral and close-packed structures, the maximum number of nearest-neighbor interactions of one molecule is 12.

Table 1
Energies of the global minimum of $(Au_{20})_N$ ($N = 2$–40) clusters and their number of the nearest-neighbor interaction.

N	E_{tot}[a]	n_{NN}[b]	N	E_{tot}[a]	n_{NN}
2	−25.506	1	22	−1089.241	32
3	−59.643	2	23	−1146.716	34
4	−99.165	3	24	−1198.550	35
5	−145.479	5	25	−1250.484	37
6	−187.901	6	26	−1304.964	38
7	−232.350	7	27	−1364.274	40
8	−283.427	9	28	−1419.580	41
9	−330.181	10	29	−1479.200	43
10	−382.729	12	30	−1545.728	45
11	−434.506	13	31	−1607.895	46
12	−490.644	15	32	−1670.106	47
13	−544.666	16	33	−1740.650	50
14	−604.098	18	34	−1792.400	52
15	−663.719	20	35	−1861.751	55
16	−727.787	21	36	−1917.172	56
17	−788.946	23	37	−1968.067	58
18	−860.958	24	38	−2020.144	60
19	−924.367	27	39	−2076.453	61
20	−980.883	30	40	−2130.684	63
21	−1036.019	31			

[a] Total energy (kJ/mol).
[b] The number of nearest-neighbor interaction.

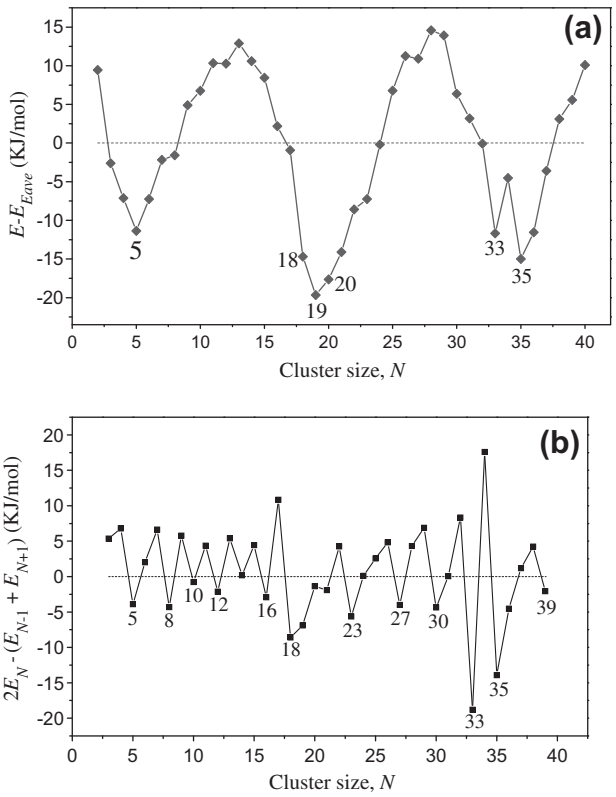

Fig. 3. (a) Plots of the energies of the global minima clusters with the MCLJ potential. E is the energy of the global minima, and E_{ave} is a four-parameter fit of the global minima: $E_{ave} = -35.77541 \times N - 212.66072 \times N^{2/3} + 649.69555 \times N^{1/3} - 444.382$ 51. Downward peaks represent the most stable magic numbers compared to the neighbors. And (b) the second energy differences (Δ_2E) of the global minima energies for the stable $(Au_{20})_N$ clusters from $(Au_{20})_2$ to $(Au_{20})_{40}$, $\Delta_2E = 2E_N - (E_{N+1} + E_{N-1})$. Peaks in Δ_2E occur for clusters which are stable compared to adjacent sizes and may correspond to "magic numbers" in the size distribution of $(Au_{20})_N$ clusters.

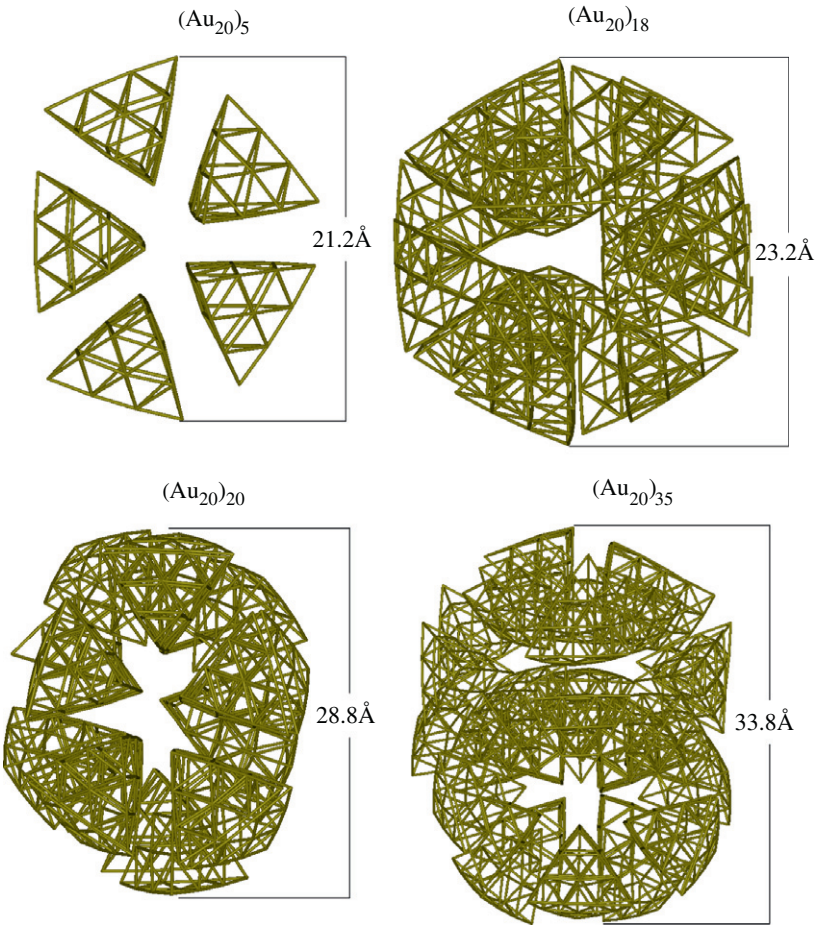

Fig. 4. The structures and dimensions of $(Au_{20})_5$, $(Au_{20})_{18}$, $(Au_{20})_{20}$ and $(Au_{20})_{35}$ clusters. Their dimensions are labeled in the figure.

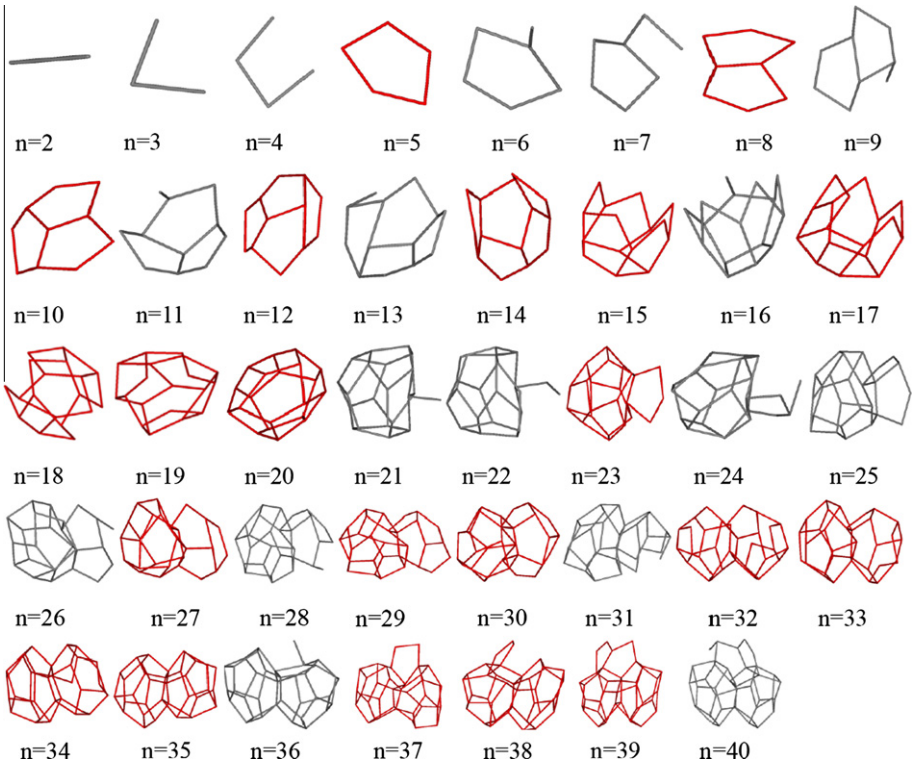

Fig. 5. Diagram of the build-up principle for $(Au_{20})_N$ clusters (N = 2–40). Sticks represent the nearest-neighbor interactions. Structures given in red represent the magic numbers with close-shell of five-membered rings.

However, the tetrahedral Au_{20} can only have four nearest-neighbor interactions, so the packing style of $(Au_{20})_N$ is much different.

Nearest-neighbor interactions plays a very important role in determining the packing style of the $(Au_{20})_N$ clusters. At the magic numbers, the nearest-neighbor interactions are in close-shell of five-membered rings. The diagram of nearest-neighbor interactions for all global minima is given in the Fig. 5, which shows the build-up principle of $(Au_{20})_N$ clusters. $(Au_{20})_N$ first grows into a five-membered ring at $N = 5$, then gradually grows to be a spherical close-shell cage at $N = 20$, next gradually grows to be a close-shell double-cage at $N = 35$, and finally tends to be a triple-cage at $N > 35$.

3.3. Discussion

At high temperature, bulk Au vaporizes into gaseous Au_N clusters, and Au_{20} is the most abundant in Au_N clusters. Vibrational spectroscopy experiments proved that the pyramidal structures for neutral Au_{20} molecule are observed in gas phase [13,17]. In this case, we can investigate the structures of $(Au_{20})_N$ molecular clusters ahead of experiments. In this work, some stable and peculiar structures were obtained, the build-up principle of $(Au_{20})_N$ clusters is very special, which is much different from some other clusters such as $(C_{60})_N$, LJ and Morse clusters.

To explain the special nature of the structure of $(Au_{20})_N$ clusters and their build-up principle, a potential analysis is carried out. The comparison among Au_{20}–Au_{20} MCLJ model potential, LJ and Morse potentials are given in Fig. 6a. It can be seen that, in the best orientation, the short-distance interaction ($R < 1$) of Au_{20}–Au_{20} potential curve is mostly to match with the Morse potential with $\rho = 11$. However, the long-distance interaction ($R > 1$) of the best orientation is much stronger than that of Morse potential (even stronger than that of the LJ potential), which may be the reason why $(Au_{20})_N$ cluster show a prominent tendency to be spherical. But for the worst orientation curve, the energy is very high in short-distance interaction, and the molecular interaction in long-distance interaction is very weak. As a comparison, the C_{60}–C_{60} MCLJ model potential and the Girifalco spherical potential [47] for C_{60} are given in Fig. 6b. It can be seen that the gap between the best and worse orientations of C_{60} MCLJ model potential is much smaller than that of Au_{20}. In other words, the orientational effect of Au_{20} molecule is much bigger than that of C_{60} molecule. This large orientation effect may be the reason why $(Au_{20})_N$ clusters hold the special build-up principle and their structures are different from other clusters.

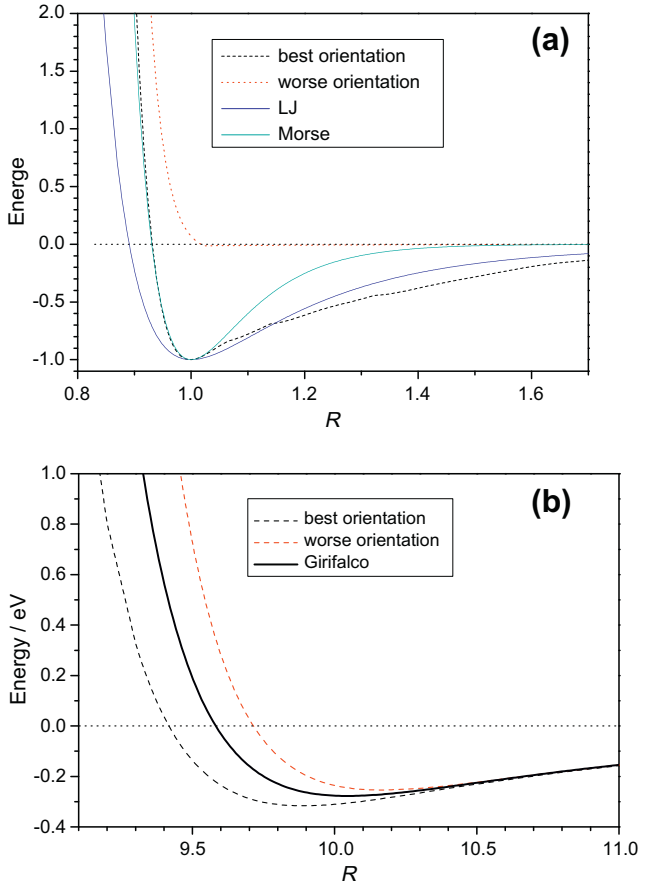

Fig. 6. (a) Comparison of Au_{20}–Au_{20} MCLJ model potential, LJ and Morse potentials with $\rho = 11$. The x-axis R is the center–center distance of two Au_{20} molecules. For easy comparison, the distance and energy are normalized. (b) Comparison of Girifalco spherical potential and C_{60}–C_{60} MCLJ model potential. R is the center–center distance between the of two C_{60} molecules. The best orientation curve represents the lowest energies at various center–center distances (molecules are in the best orientation), and the worst orientation curve represents the highest energies (molecules are in the worst orientation).

As we known, it is difficult to deal with such a complex fullerene–fullerene interaction directly by the first principle calculations. Semi-empirical potential is reasonable to give a insight for structures of large clusters (for example, MCLJ model for $(C_{60})_N$ cluster [29,43]). In this study, tetrahedral Au_{20} is simply treated as a MCLJ model, in which only the Au–Au LJ interactions between different Au_{20} molecules are considered. In previous studies, reasonable results have been obtained using such a MCLJ model for C_{60} clusters and solid [29]. Even in such a simple MCLJ model, global search of the potential energy surface of $(Au_{20})_N$ clusters is still of great difficulty. However, to make a reference, we simply calculated the binding energy of the Au_{20} dimmer (Fig. 2) using the *ab initio* method (at the MP2/cep-4G level [48,49]). The binding energy of Au_{20} dimmer of MP2 method (about −70 kJ/mol) is much larger than that of MCLJ model (−25.5 kJ/mol). Reasons for the gap of MP2 and MCLJ methods may be as follows: (1) Au–Au LJ parameters used in this study are fitted for surface, which may be not very suitable for Au_{20} clusters; (2) coulomb interactions are not concerned in our MCLJ model. Despite the fact that our MCLJ model is very rough for the Au_{20}–Au_{20} interaction, we believe that our MCLJ model can give an overall insight for the structural features of $(Au_{20})_N$ clusters. More accurate potential models for Au_{20}–Au_{20} interactions are demanded to obtain more precise results.

4. Conclusion

In summary, with the basin-hopping method and multiple-center Lennard-Jones potential, we obtained the global minimum geometries of $(Au_{20})_N$ clusters in the size range of $N = 2$–40. The energy analysis suggests some most stable magic numbers at $N = 5$, 8, 10, 12, 16, 18, 19, 20, 23, 27, 30, 33, 35. Moreover, the building-up principle of $(Au_{20})_N$ clusters is much different from other clusters. The nearest-neighbor interactions play a significant role in packing models of $(Au_{20})_N$ clusters. With the increase of cluster size N, $(Au_{20})_N$ first grow into a closed-shell five-membered ring at $N = 5$, a hollow-cage at $N = 20$, and a double-cage at $N = 35$. In addition, the orientation effect of Au_{20} molecule is much bigger than that of other molecules, and the Au_{20}–Au_{20} intermolecular potential is extremely peculiar. Finally, although our MCLJ model is very rough for the Au_{20}–Au_{20} interaction, we believe that it can give an overall insight for the structural features of $(Au_{20})_N$ clusters.

Acknowledgements

This work is financed by the National Natural Science Foundation of China (20903001), by the outstanding youth foundation of Anhui University, and by the 211 Project of Anhui University.

Appendix A. Supplementary material

Supplementary data associated with this article can be found, in the online version, at doi:10.1016/j.comptc.2012.01.024.

References

[1] G.E. Johnson, R. Mitric, V. Bonacic-Koutecky, A.W. Castleman, Clusters as model systems for investigating nanoscale oxidation catalysis, Chem. Phys. Lett. 475 (2009) 1–9.

[2] L.D. Socaciu, J. Hagen, T.M. Bernhardt, L. Woste, U. Heiz, H. Hakkinen, U. Landman, Catalytic CO oxidation by free Au_2^-: experiment and theory, J. Am. Chem. Soc. 125 (2003) 10437–10445.

[3] N. Lopez, J.K. Norskov, Catalytic CO oxidation by a gold nanoparticle: a density functional study, J. Am. Chem. Soc. 124 (2002) 11262–11263.

[4] G.J. Hutchings, M. Haruta, A golden age of catalysis: a perspective, Appl. Catal., A: General 291 (2005) 2–5.

[5] M.C. Daniel, D. Astruc, Gold nanoparticles: assembly, supramolecular chemistry, quantum-size-related properties, and applications toward biology, catalysis, and nanotechnology, Chem. Rev. 104 (2004) 293–346.

[6] F. Remacle, E.S. Kryachko, Structure and energetics of two- and three-dimensional neutral, cationic, and anionic gold clusters $Au^Z_{5\leqslant n\leqslant 9}$ ($Z = 0, \pm 1$), J. Chem. Phys. 122 (2005) 044304.

[7] N. Shao, W. Huang, Y. Gao, L.M. Wang, X. Li, L.S. Wang, X.C. Zeng, Probing the structural evolution of medium-sized gold clusters: Au_n^- ($n = 27–35$), J. Am. Chem. Soc. 132 (2010) 6596–6605.

[8] E.S. Kryachko, F. Remacle, The magic gold cluster Au_{20}, Int. J. Quantum Chem. 107 (2007) 2922–2934.

[9] Y. Gao, X.C. Zeng, Au_{42}: an alternative icosahedral golden fullerene cage, J. Am. Chem. Soc. 127 (2005) 3698–3699.

[10] W. Fa, C.F. Luo, J.M. Dong, Bulk fragment and tubelike structures of Au_N ($N = 2–26$), Phys. Rev. B 72 (2005) 205428.

[11] M.P. Johansson, D. Sundholm, J. Vaara, Au_{32}: a 24-carat golden fullerene, Angew. Chem. Int. Ed. 43 (2004) 2678–2681.

[12] X. Gu, M. Ji, S.H. Wei, X.G. Gong, Au_N clusters ($N = 32, 33, 34, 35$): cagelike structures of pure metal atoms, Phys. Rev. B 70 (2004) 205401.

[13] J. Li, X. Li, H.J. Zhai, L.S. Wang, Au_{20}: a tetrahedral cluster, Science 299 (2003) 864–867.

[14] J.L. Wang, G.H. Wang, J.J. Zhao, Density-functional study of Au_n ($n = 2–20$) clusters: lowest-energy structures and electronic properties, Phys. Rev. B 66 (2002) 035418.

[15] R.M. Olson, S. Varganov, M.S. Gordon, H. Metiu, S. Chretien, P. Piecuch, K. Kowalski, S.A. Kucharski, M. Musial, Where does the planar-to-nonplanar turnover occur in small gold clusters?, J Am. Chem. Soc. 127 (2005) 1049–1052.

[16] S. Bulusu, X.C. Zeng, Structures and relative stability of neutral gold clusters: Au-n ($n = 15–19$), J. Chem. Phys. 125 (2006) 154303.

[17] P. Gruene, D.M. Rayner, B. Redlich, A.F.G. van der Meer, J.T. Lyon, G. Meijer, A. Fielicke, Structures of neutral Au_7, Au_{19}, and Au_{20} clusters in the gas phase, Science 321 (2008) 674–676.

[18] S. Bulusu, X. Li, L.S. Wang, X.C. Zeng, Structural transitions from pyramidal to fused planar to tubular to core/shell compact in gold clusters: Au_n^- ($n = 21–25$), J. Phys. Chem. C 111 (2007) 4190–4198.

[19] W. Fa, J.M. Dong, Possible ground-state structure of Au_{26}: a highly symmetric tubelike cage, J. Chem. Phys. 124 (2006) 114310.

[20] M. Ji, X. Gu, X. Li, X.G. Gong, J. Li, L.S. Wang, Experimental and theoretical investigation of the electronic and geometrical structures of the Au_{32} cluster, Angew. Chem. Int. Ed. 44 (2005) 7119–7123.

[21] A. Yang, W. Fa, J.M. Dong, Geometrical structures and vibrational spectroscopy of medium-sized neutral Au_n ($n = 17–26$) clusters, Phys. Lett. A 374 (2010) 4506–4511.

[22] Y.L. Wang, H.J. Zhai, L. Xu, J. Li, L.S. Wang, Vibrationally resolved photoelectron spectroscopy of di-gold carbonyl clusters $Au_2(CO)_n^-$ ($n = 1–3$): experiment and theory, J. Phys. Chem. A 114 (2010) 1247–1254.

[23] E.S. Kryachko, F. Remacle, Implementation of simple logic gates on gold–ammonia bonding patterns in different charge states, Mol. Phys. (2008) 521–530.

[24] E.S. Kryachko, F. Remacle, 20-Nanogold Au_{20} (T_d) cluster and its hollow cage isomers: structural and energetic properties, J. Phys.: Conf. Series 248 (2010) 012026.

[25] J.P.K. Doye, A. Dullweber, D.J. Wales, Structural predictions for $(C_{60})_N$ clusters with an MCLJ model potential, Chem. Phys. Lett. 269 (1997) 408–412.

[26] L.J. Cheng, W.S. Cai, X.G. Shao, Geometry optimization and conformational analysis of $(C60)_N$ clusters using a dynamic lattice-searching method, ChemPhysChem 6 (2005) 261–266.

[27] J.E. Doye, D.J. Wales, The structure of $(C60)_N$ clusters, Chem. Phys. Lett. 262 (1996) 167–174.

[28] D.J. Wales, J.P.K. Doye, Global optimization by basin-hopping and the lowest energy structures of Lennard-Jones clusters containing up to 110 atoms, J. Phys. Chem. A 101 (1997) 5111–5116.

[29] F. Calvo, Thermal stability of the solidlike and liquidlike phases of $(C_{60})n$ clusters, J. Phys. Chem. B 105 (2001) 2183–2191.

[30] F. Iori, R.D. Felice, E. Molinari, S. Corni, GoIP: an atomistic force-field to describe the interaction of proteins with Au(1 1 1) surfaces in water, J. Comput. Chem. 30 (2009) 1465–1476.

[31] M. Iwamatsu, Y. Okabe, Basin hopping with occasional jumping, Chem. Phys. Lett. 399 (2004) 396–400.

[32] H.G. Kim, S.K. Choi, H.M. Lee, New algorithm in the basin hopping Monte Carlo to find the global minimum structure of unary and, binary metallic nanoclusters, J. Chem. Phys. 128 (2008) 144702.

[33] R.P. White, H.R. Mayne, An investigation of two approaches to basin hopping minimization for atomic and molecular clusters, Chem. Phys. Lett. 289 (1998) 463–468.

[34] L.X. Zhan, B. Piwowar, W.K. Liu, P.J. Hsu, S.K. Lai, J.Z.Y. Chen, Multicanonical basin hopping: a new global optimization method for complex systems, J. Chem. Phys. 120 (2004) 5536.

[35] A. Verma, A. Schug, K.H. Lee, W. Wenzel, Basin hopping simulations for MCLJ model protein folding, J. Chem. Phys. 124 (2006) 044515.

[36] L.X. Zhan, J.Z.Y. Chen, W.K. Liu, S.K. Lai, Asynchronous multicanonical basin hopping method and its application to cobalt nanoclusters, J. Chem. Phys. 122 (2005) 244707.

[37] D.J. Wales, J.P.K. Doye, A. Dullweber, M.P. Hodges, F.Y. Nakamura, F. Calvo, J. Hernández-Rojas, T.F. Middleton, The Cambridge Cluster Database (CCD). <http://www-wales.ch.cam.ac.uk/CCD.html>.

[38] C. Roberts, R.L. Johnston, N.T. Wilson, A genetic algorithm for the structural optimization of Morse clusters, Theor. Chim. Acta 104 (2000) 123–130.

[39] Y. Feng, L. Cheng, H. Liu, Putative global minimum structures of Morse clusters as a function of the range of the potential: $161 \leqslant N \leqslant 240$, J. Phys. Chem. A 113 (2009) 13651–13655.

[40] L. Cheng, J. Yang, Global minimum structures of Morse clusters as a function of the range of the potential: $81 \leqslant n \leqslant 160$, J. Phys. Chem. A 111 (2007) 5287–5293.

[41] L. Cheng, J. Yang, Modified Morse potential for unification of the pair interactions, J. Chem. Phys. 127 (2007) 124104.

[42] J. Wu, L. Cheng, Global minimum structures and structural phase diagrams of modified Morse clusters: $11 \leqslant N \leqslant 30$, J. Chem. Phys. 134 (2011) 194108.

[43] D.J. Wales, W. Branz, F. Calvo, Modeling the structure of clusters of C_{60} molecules, Phys. Rev. B 64 (2001) 235409.

[44] W. Cai, Y. Feng, X. Shao, Z. Pan, Global optimization of $(C_{60})_N$ molecular clusters, Chem. Phys. Lett. 359 (2002) 27–34.

[45] M.W. Sung, R. Kawai, J.H. Weare, Packing transitions in nanosized Li clusters, Phys. Rev. Lett. 73 (1994) 3552–3555.

[46] M. Deshpande, D. Kanhere, I. Vasiliev, R.M. Martin, Density-functional study of structural and electronic properties of Na_nLi and Li_nNa ($1 \leqslant n \leqslant 12$) clusters, Phys. Rev. A 65 (2002) 033202.

[47] L.A. Girifalco, Molecular properties of C_{60} in the gas and solid phases, J. Phys. Chem. 96 (1992) 858–861.

[48] W.J. Stevens, H. Basch, M. Krauss, Compact effective potentials and efficient shared-exponent basis sets for the first- and second-row atoms, J. Chem. Phys. 81 (1984) 6026–6033.

[49] W.J. Stevens, M. Krauss, H. Basch, P.G. Jasien, Relativistic compact effective potentials and efficient, shared-exponent basis sets for the third-, fourth-, and fifth-row atoms, Can. J. Chem. 70 (1992) 612–630.